Computational catalysis

Oxygen atom transfer catalysis: Ligand effects on the key reaction barrier in molybdenum (VI) dioxo systems[☆]

Jason M. Keith[a], Zoran D. Tomić[b], Snežana D. Zarić[c], Michael B. Hall[a,*]

[a] *Department of Chemistry, Texas A&M University, College Station, TX 77843-3255, USA*
[b] *Vinča Institute of Nuclear Sciences, Laboratory of Theoretical Physics and Condensed Matter Physics, PO Box 522, 11001 Belgrade, Serbia*
[c] *Department of Chemistry, University of Belgrade, Studentski trg 16, PO Box 158, 11001 Belgrade, Serbia*

ARTICLE INFO

ABSTRACT

Catalytic oxygen atom transfer (OAT), which frequently employs molybdenum oxo species, is an important reaction for both nature and industry. The mechanistic details of oxygen atom transfer from $Tp^RMoO_2(XPh)$ to PMe_3 were investigated for R = 3-iPr and 3-Me and X = O and S by density functional theory (DFT) calculations of the enthalpies, free energy with solvent corrections, and natural bond orbital (NBO) analysis. The mechanism for both systems proceeds via rate-determining attack of PMe_3 to form a stable intermediate with a bound $OPMe_3$ ligand. From this intermediate the reaction proceeds through a substitution involving loss of $OPMe_3$ and coordination of a single CH_3CN solvent molecule. The solvent corrected free energy barriers of the rate-determining OAT step for the O and S systems were found to be energetically more favorable for the S systems by 6.2 and 2.2 kcal/mol (for the R = 3-iPr and 3-Me, respectively). This lower energy barrier is the result of better stabilization by the SPh ligand of the Mo^{IV} products and the transition states, which are the unexpectedly later and more product-like. Additional examination of the NBO analysis emphasizes the role of the local acidity of the Mo and by extension the character of the ligands. The decreased electronegativity and softer character of the S atom result in an increased covalent character in the Mo–X bond which leads to the stabilization of a later (and lower energy) transition state and the corresponding product of the S system relative to O system.

© 2010 Elsevier B.V. All rights reserved.

1. Introduction

The transfer of O, S and N atoms from one molecule to another is a fundamental reaction in both chemistry and biology. Over the past 30 years much work has been performed to study these reactions in detail [1]. Specifically, oxygen atom transfer reactions typically involve the transfer of an O atom from a high-valent metal center accompanied by a two-electron reduction of the metal. Fig. 1 depicts the overall OAT reaction for a generic octahedral transition metal dioxo system. Catalytic OAT reactions are utilized in industrial processes such as epoxidation [2] and are involved in the function of many metalloenzymes such as cytochrome P450, sulfite oxidase, DMSO reductase and nitrate reductase.

OAT reactions involving high-valent oxo-molybdenum complexes have been repeatedly studied due to their relevance to both industrial and biological systems [3]. Both $Mo^{VI}O_2/Mo^{IV}O$ and $Mo^{VI}O/Mo^{IV}$ systems have been reported. Various supporting ligands have been utilized including complexes containing dithio-

carbamate [4], ene dithiolate [5] and hydrotris(pyrazolyl)borate (Tp) [6], while tertiary phosphines seem to be the substrate of choice in model biological systems due to their favorable solubility and tune-ability through substitution at the phosphorus [8–12].

Typically, this type of reaction, namely the attack on the M=O bond by a substrate, is described as nucleophilic attack of the substrate on the π^* molecular orbital of Mo=O leading to a reduction of the metal. Initially, it was believed that this process involved a single transition state but previous computational work on a simplified model system suggested the existence of a coordinated phosphine oxide intermediate [7]. This prediction was borne out first by the in situ detection of a corresponding coordinate intermediate [8] and later confirmed by its isolation and structural characterization [9]. Subsequently, other computational studies have predicted similar results [10].

The $Tp^RMo^{VI}O_2(XPh)$ systems selected for this study are particularly interesting. In fact, the first reported laboratory catalytic Mo complex was of this form (R = 3,5-Me, X = S) [6a]. In addition, this ligand framework allows for easy modification of the steric and electronic properties through changes in R and X. Our previous mechanistic calculations were on the $Tp^{iPr}MoO_2(OPh)$ system (using the PMe_3 as a simplified model for the experimental phosphine) in an effort to understand the entire mechanism
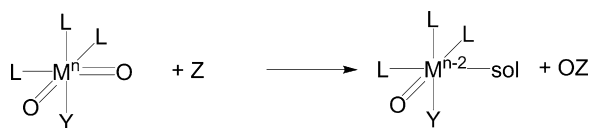
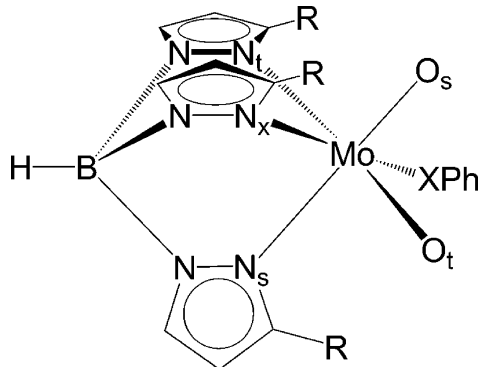**Fig. 1.** Oxygen atom transfer from a dioxo-metal to substrate Z.

Fig. 2. Atom labeling scheme.

and the corresponding kinetics of the reaction [11]. In that work it was first proposed that certain geometric features in the $O_s \cdots Mo \cdots O_t \cdots$substrate fragment in the transition state of this system could be explained as a consequence of not only nucleophilic attack of the phosphine on O, but also by simultaneous nucleophilic attack of an O lone pair on the σ^* molecular orbital of P leading to a hypervalent trigonal bipyramidal P. Herein we revisit our previously calculated mechanism for $Tp^R MoO_2(OPh) + PMe_3$ (R = iPr, Me) and compare the results directly with the corresponding $Tp^R MoO_2(SPh)$ model system. This model thiophenol complex is based on recent work by Basu and coworkers, in which $Tp^* MoO_2(S-p-R'C_6H_4)$ (R' = OMe, Me, SMe, H, Cl and CF₃) was found to be a competent catalyst for oxygen atom transfer to PMe_3 with comparable rates [12]. This result is somewhat surprising as one would hypothesize that the more electron-withdrawing OPh ligand would lead to a more positive Mo center and consequently more positive charge on the oxygen atom to be transferred making it more susceptible to a traditional nucleophilic attack.

2. Computational methodology

All calculations were performed with the hybrid DFT functional B3LYP as implemented by the Gaussian 03 programming package [13]. This functional utilizes the Becke 3-parameter exchange functional (B3) [14] combined with the correlation functional of Lee,

Yang and Parr (LYP) [15] and is known to produce good descriptions of reaction profiles for transition metal containing compounds [16,17]. Mo atoms were described using the LANL2DZ effective core potential (ECP) and basis set of Hay and Wadt [18] with the 4p orbitals replaced with the split valence functions from Couty and Hall [19]. This modified ECP basis set was further augmented with the addition of f-polarization functions (exponent = 1.043) [20]. In initial calculations P was modeled with the LANL2DZ ECP and basis set while all other atoms (H, B, C, N, O and S) were modeled using a Pople-style [21], double-ζ, 6-31G(d′,p′) basis set with polarization functions optimized for heavy atoms [22]. Subsequent calculations were performed with an all-electron basis 6-31G(d′) for P which resulted in a slight change in the relative energies with no significant change in the observed structure. Energies reported herein correspond to this larger basis set.

All geometries were fully optimized and evaluated for the correct number of imaginary frequencies through calculation of the vibrational frequencies using the analytical Hessian. Zero imaginary frequencies corresponding to an intermediate or local minimum whereas one designates a transition state or saddle point. From the analytical Hessian zero point energies as well as enthalpy and entropy corrections for 298.15 K were also calculated and added to the total electronic energy to obtain a total free energy, ΔG [298.15].

Implicit solvent effects were incorporated using the polarizable continuum model [23] with CH_3CN as the solvent using the parameter $\varepsilon = 36.64$. The solvent effects were calculated at the gas-phase geometries. The resulting solvation free energy correction including the non-electrostatic terms was added to the total free energy from above to obtain the total free energy in solvent.

In order to obtain additional insight into the difference in bonding features associated with the S and O system natural bond orbital (NBO) [24], calculations were performed on the various structures. The NBO method is a localization scheme which permits the transformation of calculated electron density into an orbital picture which is as close as possible to a classical Lewis (electron pair) description of bonding [25]. It also includes the assignments of hybridization to each atom's contribution to bond orbitals and to the lone pairs. Deviations from the Lewis-type orbitals are identified as second-order perturbations that cause the localized orbitals to mix, often this involves the transfer of electrons from occupied donor orbitals (of Lewis-type) into empty acceptor orbitals (non-Lewis orbitals). These deviations can be interpreted as a measure of electron delocalization or charge transfer, similar to the donor–acceptor interactions used to describe M–L dative bonds. Quantitative measure of the additional delocalization is expressed in terms of second-order perturbation energies [26]. By determining the occupation numbers of each localized orbital, the contribution of each atom to the orbital, and the
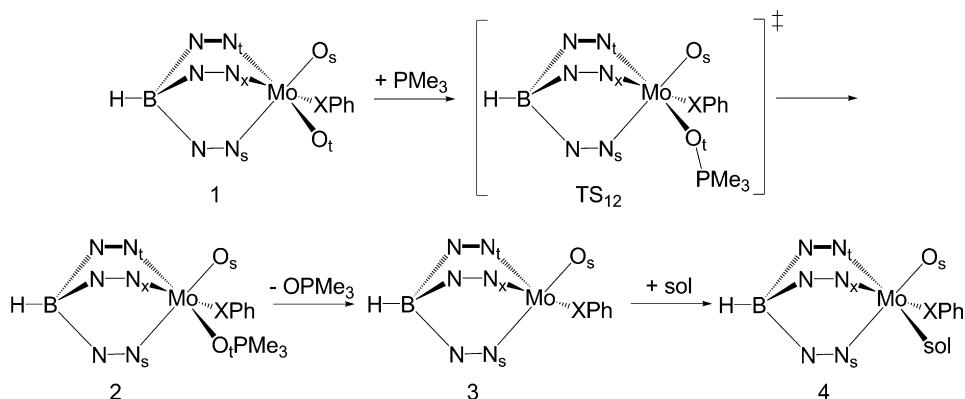

Fig. 3. Mechanistic pathway for oxygen atom transfer.

Table 1
Energies for intermediates **1**–**4** and **TS$_{12}$** (ΔH_{gas} [ΔG_{sol}], kcal/mol).

	1	TS$_{12}$	2	3	4
IsoOPh	0.00 [0.00]	12.24 [32.13]	−21.95 [−3.41]	1.03 [−1.19]	−11.93 [−1.71]
IsoSPh	0.00 [0.00]	8.99 [25.9]	−29.81 [−13.85]	−4.13 [−7.97]	−24.13 [−14.10]
MeOPh	0.00 [0.00]	12.87 [29.60]	−20.76 [−5.39]	1.68 [−1.49]	−12.50 [−3.50]
MeSPh	0.00 [0.00]	10.44 [27.44]	−27.81 [−12.73]	−0.68 [−1.40]	−22.38 [−11.71]

second-order mixing of orbitals, the NBO method identifies the most prominent Lewis description and suggests the origin of the most important deviations: such as the donor–acceptor interactions and other mixing that suggest the importance of other Lewis resonance structures. Core electrons should have no effect on NBO calculations that by definition focus on the valence electrons involved in bonding therefore additional NBO calculations were not performed for the results from the calculations with the

all-electron basis set on P. NBO results from the isopropyl and methyl are virtually indistinguishable so only the isopropyl are described.

Fig. 2 illustrates the labeling scheme used throughout this work. The O atom subscripts differentiate between the spectator O (labeled O$_s$), the O to be transferred (labeled O$_t$) and the O from the OPh ligand (O$_{Ph}$) while the subscripts of nitrogen atoms indicate the ligand in the respective *trans* position (N$_s$ *trans* to O$_s$, N$_t$
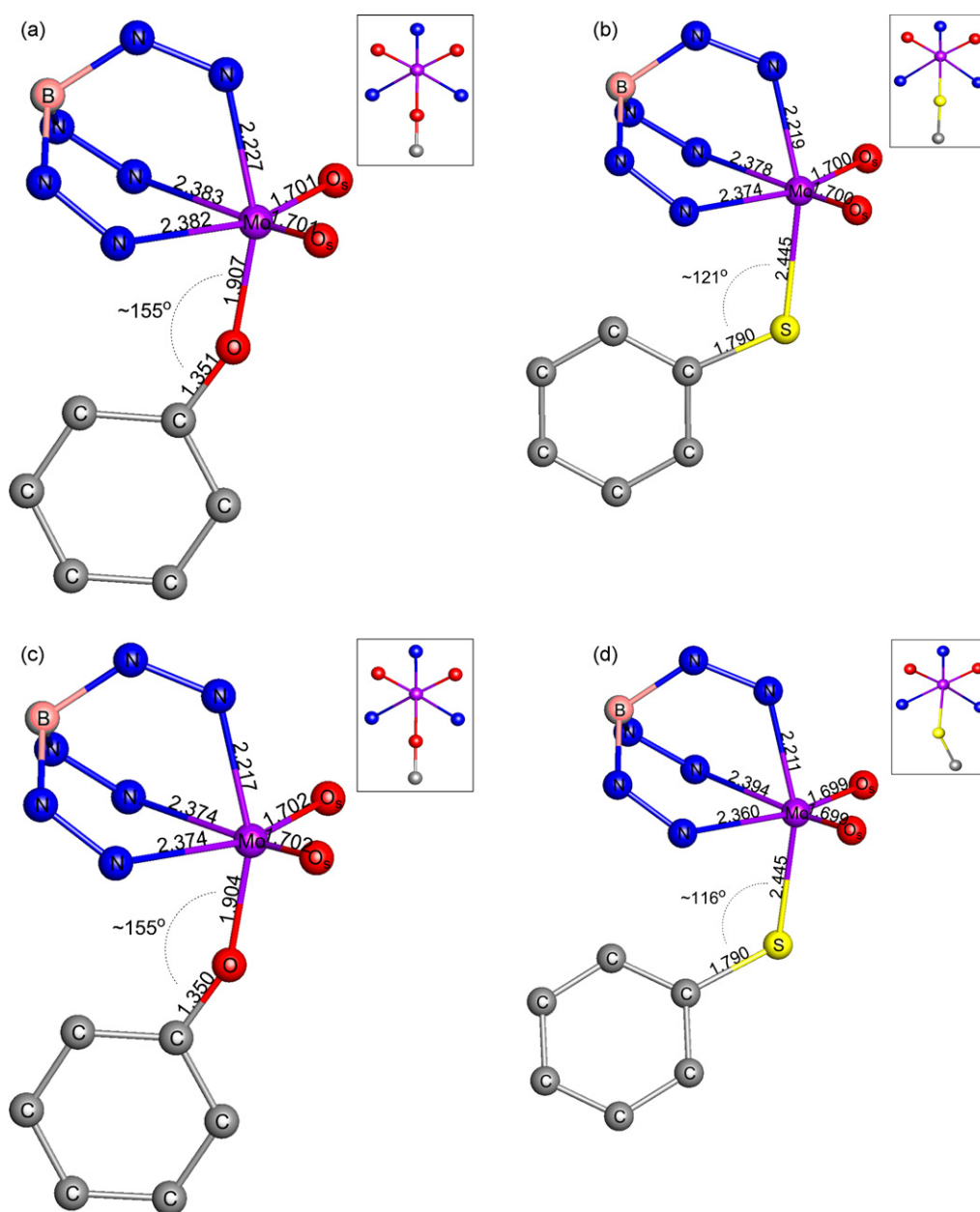

Fig. 4. Geometries for species **1** for (a) IsoOPh; (b) IsoSPh; (c) MeOPh; (d) MeSPh. All H atoms as well as C atoms on the Tp^R ligand were omitted from the images for simplicity. View down the Mo–B axis shown in upper right corner of each structure.

Fig. 5. Transition state geometries for **TS$_{12}$** for (a) IsoOPh; (b) IsoSPh; (c) MeOPh; (d) MeSPh. All H atoms as well as C atoms on the Tp^R ligand were omitted from the images for simplicity. View down the Mo–B axis shown in upper right corner of each structure.
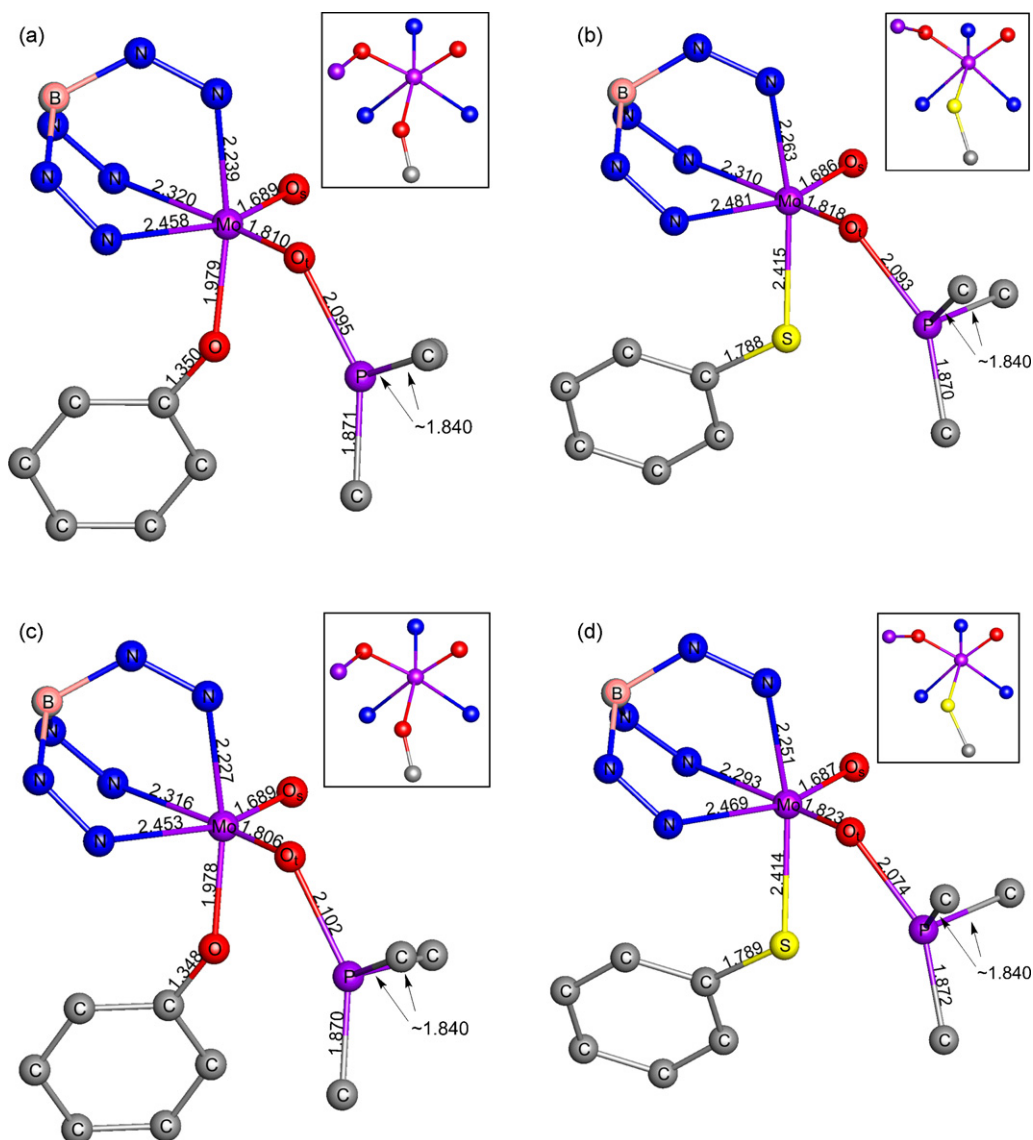
trans to O$_t$ and N$_x$ *trans* to XPh). The methyl and isopropyl versions of the O and S system will be referred to as MeOPh, IsoOPh, MeSPh and IsoSPh.

3. Results and discussion

3.1. Reaction profile

The calculated minimum energy pathway for all four systems is analogous to that of our previous study on IsoOPh system [11] and is presented in Fig. 3. This mechanism proceeds first from species **1** through the attack of PMe$_3$ to form a stable intermediate with a bound OPMe$_3$ ligand, species **2**. From **2** the reaction involves a substitution involving loss of OPMe$_3$ and the coordination of a single CH$_3$CN solvent molecule. While our previous mechanistic examination of the O system found this process to be dissociative involving the coordinatively unsaturated intermediate **3** [11] recent experimental results for the S system suggest an associative process [12]. Energies for these intermediates as well as for the transition state between species **1** and **2**, **TS$_{12}$**, are presented in Table 1. From species **3** the association of OPMe$_3$ or CH$_3$CN to

form **2** or **4** is exothermic and found to be enthalpically barrierless. Entropic barriers for these processes do exist but are difficult to quantify and were discussed previously in detail [11]. Comparison between the associative and dissociative pathways of the O and S system have no effect on the overall rates of these reactions and where thus determined to be beyond the scope of this study and will not be examined here. In general, our results indicate that $\Delta G^{\ddagger}$ for the S systems are lower in energy than the corresponding O system ($\Delta\Delta G^{\ddagger}$ = 6.2 and 2.2 kcal/mol for *i*Pr and Me systems). Experimental free energy barriers were determined to be ~22 kcal/mol for Tp^{iPr}MoO$_2$(OPh) with PEt$_3$ [11] and for Tp*MoO$_2$(SPh) with PMe$_3$ [12], while the enthalpic barriers were about 1 kcal/mol lower for the sulfur case.

Geometries for species **1** vary with respect to the XPh ligand (Fig. 4). Due to the larger atomic radius of S, the Mo–X and X–C bond lengths are significantly longer for the S system (~2.4 and ~1.8 Å for S; ~1.9 and ~1.4 Å for O). There is also a significant decrease in the Mo–X–C bond angle down from ~155° in the O system to ~120° for the S. This decrease is most likely caused by a decrease in the hybridization of S compared to O similar to the difference between H$_2$O (~105°) and H$_2$S (~92°). Generally, the decrease in
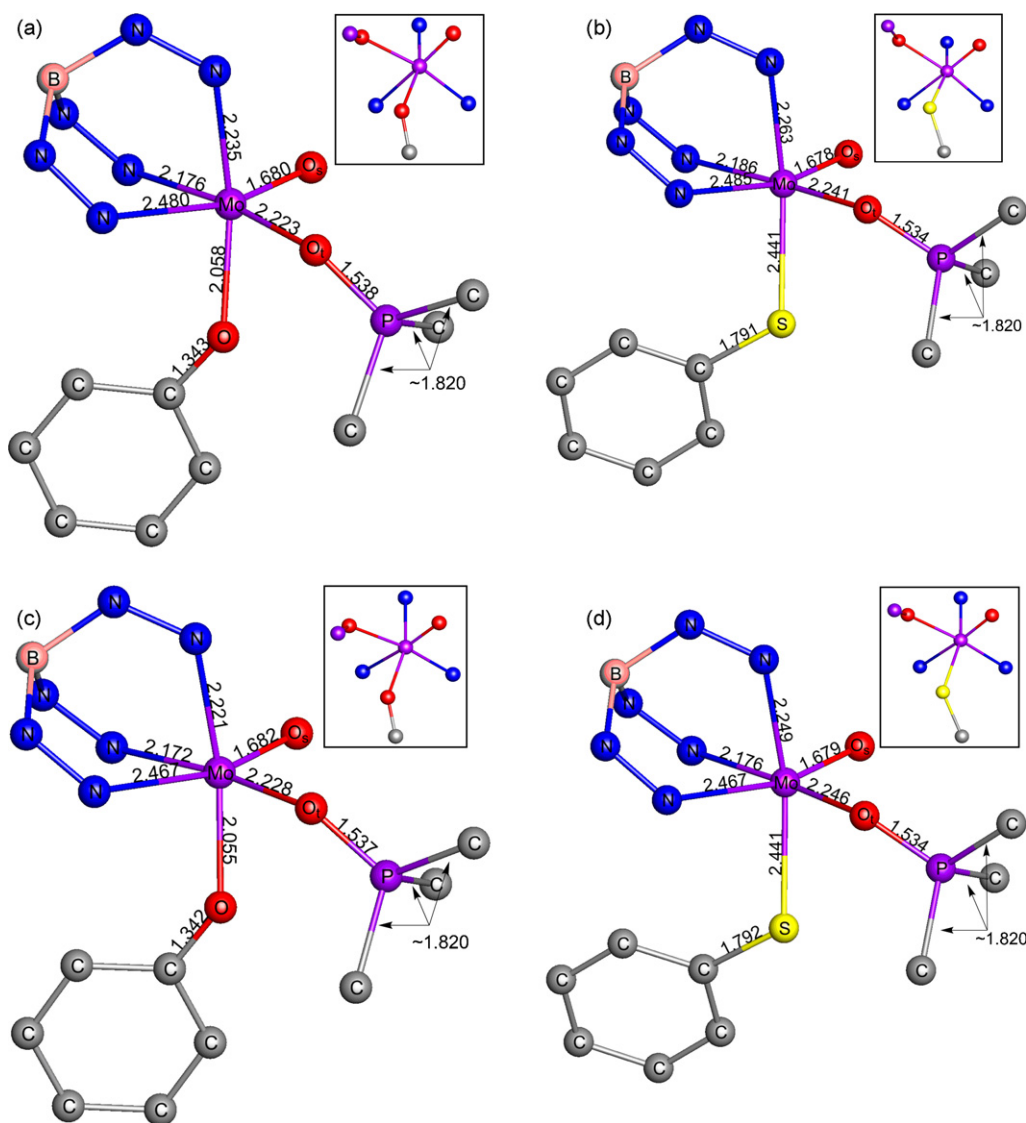
Fig. 6. Geometries for species **2** for (a) IsoOPh; (b) IsoSPh; (c) MeOPh; (d) MeSPh. All H atoms as well as C atoms on the Tp^R ligand were omitted from the images for simplicity. View down the Mo–B axis shown in upper right corner of each structure.

overlap of the ns atomic orbital on X in the Mo–X and X–C bonding orbitals when switching from O to S drives this decrease in hybridization. With respect to how these changes affect the other bonds, the increase in the Mo–N_x bonds by 0.02–0.03 Å in the S system suggests that the Mo–S bond has increased its covalent bonding character compared to the Mo–O_{Ph} bond therefore lengthening the Mo–N_x bond due to the increased *trans* influence. Further examination of the Mo–X bonding interactions and their consequences are discussed in Section 3.3.

An additional noteworthy difference in these systems is that the enthalpies of the O system seem to be fairly independent of the R group while the S system demonstrates an increase of the relative enthalpies of intermediates **2**–**4** and **TS$_{12}$** with respect to **1** for R = Me compared to *i*Pr. We believe this difference arises from the difference in bonding. In the O system the OPh ligand is bound to the metal through a dative bond and the orientation of the OPh moiety is determined purely by steric factors, thus OPh lies in the σ-plane. In the S system the covalent Mo–S bond is actually stabilized by distortion from the mirror plane and the longer Mo–S bond decrease the steric interactions between XPh and R. This is apparent in the MeSPh structure in Fig. 4. For IsoSPh however, the increased steric bulk of the *i*Pr groups still dominates forcing SPh

into the mirror plane and resulting in a destabilization of species **1**.

Fig. 5 shows details of the structures for **TS$_{12}$** for all four systems examined. As mentioned in previous work, this transition-state geometry suggests a concurrent nucleophilic attack of the lone pair on PMe$_3$ upon the π* molecular orbital of Mo–O_t and nucleophilic attack of a O_t lone pair on the σ* molecular orbital of P. This simultaneous process is suggested by the geometry of the P moiety in the transition state, where the phosphorus is in a hypervalent geometry as a pseudo-trigonal bipyramid with the P lone pair residing in the equatorial plane (seesaw type structure), significantly distorted from the tetrahedral geometry expected from a simple nucleophilic attack by the lone pair on PMe$_3$. In all four species two of the X–P–C bonds are small (~95°) while the third is larger (~150°). In addition the three P–C bond lengths are not equivalent; the P–C bond *trans* to O_t is ~0.03 Å longer, consistent with partial formation of a 3-center, 4-electron bond.

While the distorted P geometry exists in all four systems there are important differences in the geometry of this transition state between the O and S systems. Firstly, the Mo–O_t bonds in the S systems are longer by 0.008 (*i*Pr) and 0.017 Å (Me). Accordingly, the O_t–P distance for these systems has decreased by 0.002 (*i*Pr)

and 0.028 Å (Me). These differences indicate a *later* transition state, while the increased stabilization of the transition state and products for the SPh systems would have suggest an *earlier* transition state by the Hammond postulate. This nontraditional behavior is a result of the specific bonding interactions of the SPh ligand which act to stabilize the attack of the PMe_3 and move the transition state both later and lower in energy. For instance, the $Mo-O_{Ph}$ (dative bond) distance increases by ~0.08 Å from **1** to **TS_{12}** while the Mo–S (covalent bond) distance *decreases* by ~0.03 Å. Further examination of this will be discussed further in Section 3.3.

Following attack of PMe_3, the reaction proceeds to intermediate **2**, formally an octahedral Mo^{IV} with a bound O_tPMe_3 ligand. Free energies indicate a significantly higher stabilization of this species compared to **1** for the S system. Geometries for species **2** are presented in Fig. 6. The distorted P geometry observed in the transition state is no longer present as the geometry at the P atom is now pseudo-tetrahedral with all three P–C distances and all three O_t–P–C angles approximately equal. The new P–C distances are consistent with free O_tPMe_3, while the $P-O_t$ distance is slightly elongated from what is calculated for free O_tPMe_3 (1.50 Å). The $Mo-O_t$ distances in the S system are longer by ~0.02 Å than those in the O systems while the O_t–P distances for the S system are only ~0.003 Å smaller. The behavior of the Mo–XPh interaction continues to differ for $X = O_{Ph}$ and S. From **TS_{12}** the $Mo-O_{Ph}$ (dative bond) distance has continued to increase by an additional ~0.08 Å. By contrast the Mo–S (covalent bond) distance has increased from **TS_{12}** by only ~0.026 Å, which brings it back to ~2.44 Å as in species **1**. This versatility in the S system arises from covalent nature of the Mo–S bond that allows electrons to flow between the two atoms while the mostly ionic (dative) $Mo-O_{Ph}$ bond is dominated by the electrostatic forces. In the O system as the Mo is reduced (decreasing the positive charge) the ionic attraction decreases and the bond length increases. Interestingly, the XPh group is bent away from the PMe_3 moiety in **TS_{12}** and species **2** for all systems illustrating the increased steric interactions. Further examination of this will be provided in Section 3.3.

From species **2** the reaction proceeds through a ligand exchange between O_tPMe_3 and CH_3CN. The differences apparent in the energies and geometries between the O and S systems in species **3** and **4** resemble those of species **2** and will not be discussed further here. A further examination of the bonding will be discussed in Section 3.3.

3.2. Natural population analysis

In addition to the examination of the potential energy surface and the structure of the various reaction species discussed above, an examination of the charge distribution throughout the reaction profile is especially informative. Atomic charges were calculated using natural population analysis (NPA). The results for the IsoXPh systems are depicted in Fig. 7, which illustrates the prominent characteristics of the NPA charge variations and differences between the O and S systems for the Mo, O_s, O_t and X atoms. It is noteworthy that despite a difference in charges on individual atoms for the two systems the variation of these charges throughout each reaction mirrors one another. Thus, not only are the shapes of the plots similar, but also the differences between the successive steps. This parallel behavior suggests that the nature of the individual steps in the mechanism are essentially the same and in accordance with the previously proposed mechanism. The largest difference in charges between the atoms in the two systems is, not surprisingly, that of the X atom itself. The charge on S is significantly less negative in accordance with its decreased electronegativity. It should also be pointed out that the calculated charges on the Mo atoms in all reaction species are significantly lower than what would be predicted by the formal charges. Thus, significant ligand to metal electron
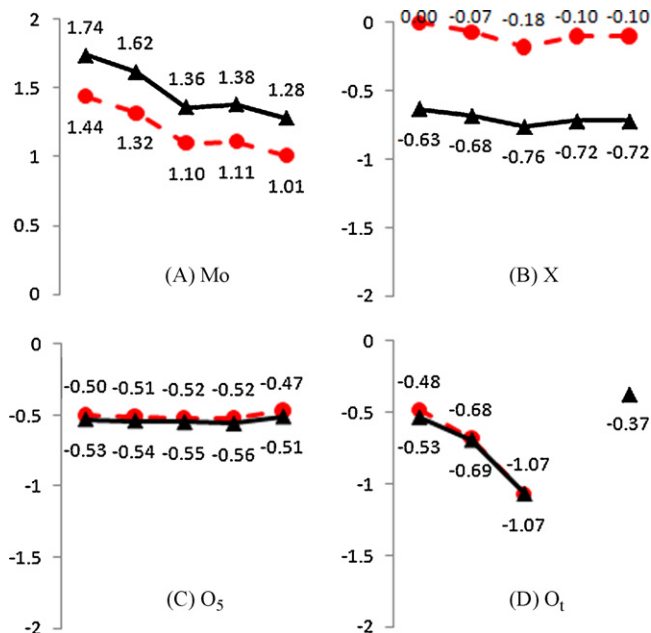

Fig. 7. NPA charge variations in the O system (▲ and solid line) and S system (● and dashed line) for (a) Mo; (b) X; (c) O_s; (d) O_t. The 5 points correspond to species **1**, **TS_{12}**, **2**, **3** and **4** respectively (plot d species **3** and **4** correspond to free O_tPMe_3 for both systems, redundant species have been omitted for simplicity).

transfer exists and increases as the reaction proceeds (indicated by the downward trend of the charge on Mo). In accordance with the less negative charge on S compared to O_{Ph}, the Mo has a smaller positive charge in the SPh system. Unexpectedly, the charges on O_s and O_t are also lower in S system indicating that all ligands are donating more charge to the Mo, but in this case the differences are small. As would be expected in species **1** the charge on O_s and O_t are similar to each other in both systems with values of ~0.53 and ~0.49 in the O and S system. For the purposes of Fig. 7 the O atom to be transferred (O_t) in the S system is assumed to be the atom with the slightly lower (more positive) charge consistent with it being the site of nucleophilic attack. All of this information taken together suggests that for both the O and S systems the process of attack of the incoming ligands, and the subsequent bonding to oxygen is associated with the transfer of electrons to Mo from O_t as expected from the formal two electron reduction of Mo.

3.3. Natural bond orbitals

The calculated electron density from the DFT calculations was transformed into Lewis and non-Lewis-type natural bond orbitals (NBO). Using the NBO terminology, the Lewis-type orbitals are designated as bonding (BD) and lone pair (LP) orbitals, while the non-Lewis orbitals are designated as anti-bonding (BD*) and lone pair (LP*) orbitals [27]. To obtain quantifiable insight into dative bonding further examination of the pattern of the interactions between the Lewis-type and non-Lewis-type orbitals can be utilized. The magnitude of these stabilization energies is expressed by the values of second-order perturbation energies. While the occupancies, energies, and hybridization of the NBOs and all of the mixing (donor–acceptor) interactions relevant for the description of bonding have been saved for supplementary material, the main bonding features relevant to the metal center are schematically presented in Fig. 8 (left: IsoOPh; right: IsoSPh) and are described below. The important non-Lewis orbitals are marked with asterisk (*). Every covalent bond (depicted by a single line) has associated with it a corresponding anti-bonding orbital.
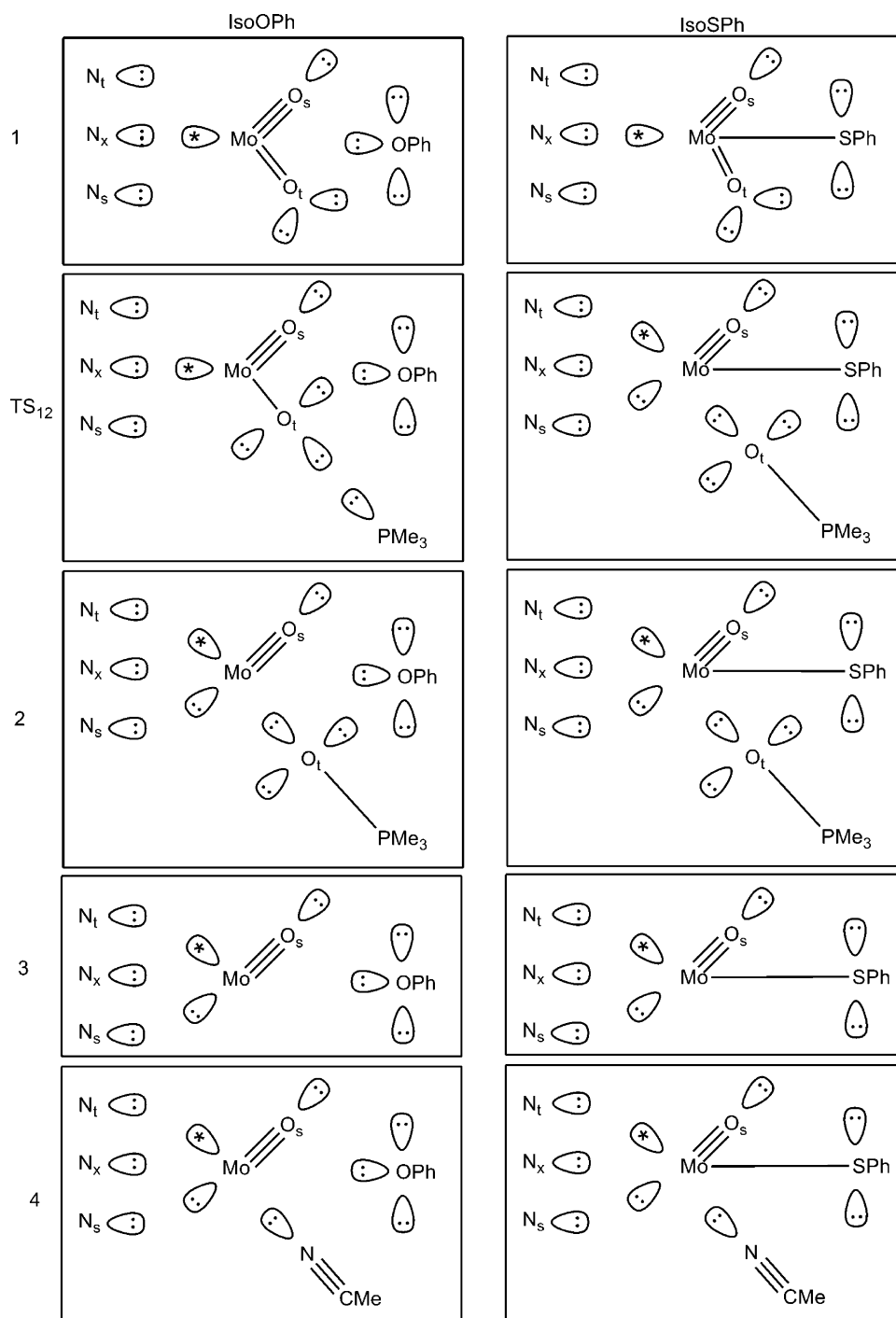
Fig. 8. Schematic description of NBO's relevant for the bonding of ligands to Mo in O system. Bonds (NBO BD's) are represented with a single line (−), Lewis lone pairs (NBO LP's) are represented with a filled lobe (⊙) and non-Lewis orbitals are represented by a starred lobe (✳) representing a combination of low occupancy non-Lewis lone pairs (LP*) and anti-bonding orbitals (BD*) with large Mo components with a total occupancy of ∼2 electrons.

Examination of the NBO description of species **1** reveals one dramatic difference between the O and S systems which is maintained throughout the reaction. For the O system a Mo–O$_{Ph}$ covalent bond was not detected by NBO method indicating a predominant dative-type interaction (more electrostatic). In the NBO model this is illustrated by the presence of three O$_{Ph}$ LP orbitals and a significant donor–acceptor interaction between one of these filled O$_{Ph}$ LP orbitals and a partially filled Mo LP* orbital. In contrast to this, for the S system a Mo–S covalent bond is present (represented with a solid line) which indicates more substantial mixing between the Mo and the S hybrids that leads the significant difference in the Mo–X

bond in these two systems. As expected the Tp ligand is bound to Mo through three predominantly ionic-type (dative) bonds. These bonds are expressed in the NBO description as charge transfer from the filled LP orbitals located on the N to the non-Lewis orbitals predominantly located on the metal and are consistent throughout the reaction. For clarification it should be pointed out that the NBO calculations (and the corresponding diagrams) for species **1** represent only one of two possible resonance structures with respect to Mo–O$_t$ and Mo–O$_s$ and that the difference represented by the single structure is not significant. In fact, one of the largest second-order perturbation energies for species **1** is a donation from one

of the partially filled Mo–O_t anti-bonding orbitals to one of the Mo–O_s anti-bonding orbitals, a mixing that leads toward the other resonance form and the equilibration of the two bonding interactions. This equalization of the two resonance structures necessarily appears in the NBO analysis as both resonance structures contribute equally in the DFT calculations.

Proceeding to **TS$_{12}$** a second significant difference between the two systems is apparent; **TS$_{12}$** differs with respect to the Mo–O_t and O_t–P interactions in the two systems. In the OPh system the number of covalent bonds between Mo and O_t has only decreased from two to one indicating that O_t is still bound to Mo covalently while the O_t–P bond has not formed but there is significant donor–acceptor interaction between the filled P LP orbital and one of the Mo–O_t BD* (π^*) orbitals demonstrating that the interaction between the Mo–O_t and the PMe$_3$ is still predominantly electrostatic. In the SPh system however, the Mo–O_t bond order has decreased to zero such that there is no longer any covalent bonding character remaining between the Mo and O_t. In addition, the O_t–P covalent bond is already formed. This difference is indicative of a *later* transition state as was also observed in the geometric structures (*vide supra*). It is this change in the electronic structure that resolves the unexpected *lower* reaction barrier (TS) in the S system as discussed above in Section 3.1.

As discussed in Section 3.2 the pattern of charge variation along the reaction coordinate on Mo in both O and S system is similar with Mo in S system being more negative. Closer inspection of the NBO analysis demonstrates that in all reaction species starting with species **TS$_{12}$** there is shift of electron density toward occupation of lone pair orbitals (both LP and LP*) located on Mo for both systems. This redistribution of the electrons is the primary contribution to the decrease in charge on the Mo and is related to the formal two-electron reduction of the Mo. This can be seen as the direct result of the attack of phosphine ligand upon O_t and it is in accordance with the variation of NPA charges which indicates donation of electrons from ligands to Mo.

Closer inspection of the changes in the NBO description corresponding to the charge transfer and the energies associated with them in **TS$_{12}$** suggests that the charge donation to Mo and increase in the occupancy of Lewis and non-Lewis lone pair orbitals has a different source for the two systems. In the O system the main contribution of this redistribution in **TS$_{12}$** comes from the loss of one of the Mo–O_t bond and the resulting conversion of the corresponding BD and BD* orbitals to an O_t LP orbital and a Mo LP* orbital. While this is also observed in the S system, the most significant change in this system is the formation of a new filled LP orbital on Mo. This new Mo LP orbital does not appear in the O system until the Mo–O_t covalent bond has been completely broken in species **2**. Thus, in the S system the Mo center in **TS$_{12}$** has already been fully reduced through the transfer of two electrons from the Mo–O_t bond, while in the O system the reduction has only begun. This later transition state is stabilized in the S system through a strong interaction associated with donation of electrons from the non-Lewis lone pair orbitals on Mo to the Mo–S anti-bonding orbital thus strengthening the Mo–S bond (which was apparent when evaluating the Mo–S bond lengths in Section 3.1). Overall this means that the covalent character of the Mo–S bond allows it to modulate the interaction between the Mo and the S strengthening the bond in order to stabilize the later transition state.

As discussed above this reaction can be seen as simultaneous nucleophilic attack of PMe$_3$ on O_t and of O_t on the P. Evaluation of the NBO's relevant for the formation of **TS$_{12}$** should help differentiate between these two processes. The orbital picture obtained by NBO method partially describes the formation of O_t–P bond in **TS$_{12}$** of the O system and the transfer of electrons from a lone pair orbital on P to the anti-bonding Mo–O_t orbital (standard nucleophilic attack of the P lone pair on the O_t π^* orbital) and simultaneous

transfer of electrons from a lone pair orbital on O_t to the lone pair orbital on P accompanied with electron transfer from that P lone pair orbital to one of the anti-bonding P–C orbitals (nucleophilic attack of the O_t lone pair on the P σ^* orbital). This is expected to weaken the corresponding P–C bond; thus, to explain the difference in the calculated P–C bond lengths in the phosphine fragment of **TS$_{12}$** discussed in Section 3.1. This process is coupled with the transfer of electrons to the non-Lewis lone pair on Mo. In **TS$_{12}$** of the S system however, neither of these interactions can be seen in the NBO analysis as the O_t–P covalent bond has already formed (in essence these concurrent nucleophilic attacks have already occurred).

In species **2** the NBO orbitals for the two systems are similar with no Mo–O_t covalent bonds. Instead a dative bond exists between the O_t LP orbital and Mo LP* orbital. In addition the O_t–P covalent bond is fully formed for both systems. The Mo–X interactions are still different with a covalent Mo–S bond and a dative Mo–O_{Ph} bond and they remain so throughout the reaction as illustrated in Fig. 6.

4. Conclusion

The mechanistic details of oxygen atom transfer from Tp^{R}MoO$_2$(XPh) to PMe$_3$ were investigated for X = O_{Ph} and S. Independent of R group the rate-determining step was the attack of PMe$_3$ to form a stable intermediate with a bound OPMe$_3$ ligand. The transition state for this process consists of nucleophilic attack of the substrate on the π^* molecular orbital of Mo=O_t coupled with simultaneous nucleophilic attack of an O_t lone pair on the σ^* molecular orbital of P leading to a hypervalent pseudo-trigonal bipyramidal P in the transition state. Detailed examination of the structures including a natural bond order analysis performed on this transition state support this description. From the resulting intermediate the reaction proceeds through a ligand exchange process involving loss of O_tPMe$_3$ and coordination of a single CH$_3$CN solvent molecule.

Results of the NBO analysis suggest that local acidity (ease of reduction) of the Mo, which makes it capable of accepting electrons, is an important factor for driving this reaction. However, the effect of this electron transfer on the stability of the whole system depends on the character of the ligands. The decreased electronegativity of the S atom leads to more covalent bonding character for the Mo–X bond when compared to O, a difference which has a direct impact on the rates of the reactions. The barriers for the O and S systems were found to differ energetically with $\Delta\Delta G^{\ddagger} = 6.2$ and 2.2 kcal/mol (for the R = iPr and Me, respectively) in favor of the S system. This lower energy is the result of stabilization of the transition state and the Mo^{IV} products by the SPh ligand which was found to modulate the Mo–S interaction throughout the process. In the transition state the Mo–S bond strengthened in order to accommodate the reduced metal center allowing for a later, more product-like, transition state thus lowering the energy. In effect the covalent Mo–S bond was more versatile throughout the reaction adjusting to stabilize the oxidation state of the metal while in the O system the Mo–O_{Ph} interaction was dominated by electrostatic forces resulting in a monotonic increase of the Mo–O_{Ph} bond from **1** through **TS$_{12}$** to **2**.

Acknowledgements

Appendix A. Supplementary data

Supplementary data associated with this article can be found, in the online version, at doi:10.1016/j.molcata.2010.02.027.

References

[1] (a) H. Taube, ACS Symp. Ser. 198 (1982) 151;
(b) K.B. Sharpless, Tetrahedron 50 (1994) 4235;
(c) R.H. Holm, Chem. Rev. 87 (1987) 1401;
(d) L.K. Woo, Chem. Rev. 93 (1993) 1125;
(e) J.H. Espenson, Adv. Inorg. Chem. 54 (2003) 157.
[2] (a) B.S. Lane, K. Burgess, Chem. Rev. 103 (2003) 2457;
(b) W.A. Nugent, T.V. RajanBabu, M.J. Burk, Science 259 (1993) 479.
[3] (a) R.H. Holm, Coord. Chem. Rev. 100 (1990) 183;
(b) J.H. Enemark, C.G. Young, Adv. Inorg. Chem. 40 (1993) 1;
(c) J.H. Enemark, J.J.A. Cooney, J.-J. Wang, R.H. Holm, Chem. Rev. 104 (2004) 1175;
(d) C.G. Young, in: B. Meunier (Ed.), Biomimetic Oxid. Catal. Transition Met. Complexes, Imperial College Press, 2000, pp. 415–459 (Chapter 9).
[4] (a) R. Barral, C. Bocard, I. Seree de Roch, L. Sajus, Tetrahedron Lett. (1972) 1693;
(b) M.S. Reynolds, J.M. Berg, R.H. Holm, Inorg. Chem. 23 (1984) 3057.
[5] (a) S.K. Das, P.K. Chaudhury, D. Biswas, S. Sarkar, J. Am. Chem. Soc. 116 (1994) 9061;
(b) H. Oku, N. Ueyama, M. Kondo, A. Nakamura, Inorg. Chem. 33 (1994) 209;
(c) K.-M. Sung, R.H. Holm, J. Am. Chem. Soc. 124 (2002) 4312;
(d) K.-M. Sung, R.H. Holm, J. Am. Chem. Soc. 123 (2001) 1931;
(e) J.P. Donahue, C.R. Goldsmith, U. Nadiminti, R.H. Holm, J. Am. Chem. Soc. 120 (1998) 12869;
(f) B.S. Lim, R.H. Holm, J. Am. Chem. Soc. 123 (2001) 1920.
[6] (a) Z. Xiao, C.G. Young, J.H. Enemark, A.G. Wedd, J. Am. Chem. Soc. 114 (1992) 9194;
(b) Z. Xiao, M.A. Bruck, J.H. Enemark, C.G. Young, A.G. Wedd, Inorg. Chem. 35 (1996) 7508;
(c) V.N. Nemykin, S.R. Davie, S. Mondal, N. Rubie, M.L. Kirk, A. Somogyi, P. Basu, J. Am. Chem. Soc. 124 (2002) 756.
[7] (a) M.A. Pietsch, M.B. Hall, Inorg. Chem. 35 (1996) 1273;
(b) S.D. Zarić, M.B. Hall, in: L. Banci, P. Comba (Eds.), NATO ASI Series, Kluwer Academic Publishers, Boston, 1997, p. 255.
[8] P.D. Smith, A.J. Millar, C.G. Young, A. Ghosh, P. Basu, J. Am. Chem. Soc. 122 (2000) 9298.
[9] (a) A.J. Millar, C.J. Doonan, P.D. Smith, V.N. Nemykin, P. Basu, C.G. Young, Chem. Eur. J. 11 (2005) 3255;
(b) C.J. Doonan, A.J. Millar, D.J. Nielsen, C.G. Young, Inorg. Chem. 44 (2005) 4506;
(c) V.N. Nemykin, J. Laskin, P. Basu, J. Am. Chem. Soc. 126 (2004) 8604;
(d) V.N. Nemykin, P. Basu, Inorg. Chem. 44 (2005) 7494.
[10] (a) C.E. Webster, M.B. Hall, J. Am. Chem. Soc. 123 (2001) 5820;
(b) A. Thapper, R.J. Deeth, E. Nordlander, Inorg. Chem. 41 (2000) 6695;
(c) L.M. Thompson, M.B. Hall, J. Am. Chem. Soc. 123 (2001) 3995;
(d) A. Žmirić, S.D. Zarić, Inorg. Chem. Commun. 6 (2002) 446.
[11] B.W. Kail, L.M. Perez, S.D. Zarić, A.J. Millar, C.G. Young, M.B. Hall, P. Basu, Chem. Eur. J. 12 (2006) 7501.
[12] (a) R.S. Sengar, V.N. Nemykin, P. Basu, J. Inorg. Biochem. 102 (2008) 748;
(b) P. Basu, V.N. Nemykin, R.S. Sengar, Inorg. Chem. 48 (2009) 6303.
[13] M.J. Frisch, et al., Gaussian 03, Revision E.01, Gaussian, Inc., Pittsburgh, PA, USA, 2003.
[14] A.D. Becke, J. Chem. Phys. 98 (1993) 5648.
[15] C. Lee, W. Yang, R.G. Parr, Phys. Rev. B 37 (1988) 785.
[16] J. Baker, M. Muir, J. Andzelm, A. Scheiner, in: B.B. Laird, R.B. Ross, T. Ziegler (Eds.), Chemical Applications of Density-Functional Theory, ACS Symposium Series 629, American Chemical Society, Washington, DC, 1996.
[17] S. Niu, M.B. Hall, Chem. Rev. 100 (2000) 353.
[18] P.J. Hay, W.R. Wadt, J. Chem. Phys. 82 (1985) 299.
[19] M. Couty, M.B. Hall, J. Comput. Chem. 17 (1996) 1359.
[20] A.W. Ehlers, M. Böhme, S. Dapprich, A. Gobbi, A. Höllwarth, V. Jonas, K.F. Köhler, R. Stegmann, A. Veldkamp, G. Frenking, Chem. Phys. Lett. 208 (1993) 111.
[21] (a) P.C. Hariharan, J.A. Pople, Chem. Phys. Lett. 16 (1972) 217;
(b) M.M. Francl, W.J. Pietro, W.J. Hehre, J.S. Binkley, M.S. Gordon, D.J. DeFrees, J.A. Pople, J. Chem. Phys. 77 (1982) 3654.
[22] R. Krishnan, J.S. Binkley, R. Seeger, J.A. Pople, J. Chem. Phys. 72 (1980) 650.
[23] J. Tomasi, B. Mennucci, R. Cammi, Chem. Rev. 105 (2005) 2999.
[24] E.D. Glendening, A.E. Reed, J.E. Carpenter, F. Weinhold, NBO Version 3.1, University of Wisconsin, Madison, WI (1990).
[25] F. Weinhold, C.R. Landis, Chem. Ed.: Res. Pract. Eur. 2 (2001) 91.
[26] F.J. Weinhold, Chem. Ed. 76 (1999) 1141.
[27] For further clarification Lewis lone-pair orbitals (LP) are localized (directional) orbitals often with significant p character while non-Lewis lone-pair orbitals (LP*) are delocalized orbitals primarily made up of s and d character.